COMPARISON OF UAV LIDAR AND IMAGERY FOR BEACH MONITORING

L. Shaw [1,2], P. Helmholz[1]*, D. Belton [1], N.Addy [2]

[1] Spatial Sciences, Curtin University, GPO Box U1987, Perth WA 6845, Australia - (Petra.Helmholz, D.Belton)@curtin.edu.au
[2] Land Surveys, 19 Brennan Way, Belmont WA 6104, Australia – (LShaw, NAddy)@landsurveys.net.au

Commission I, ICWG I/II

KEY WORDS: Beach Monitoring, UAV, LiDAR, Photogrammetry, Evaluation

ABSTRACT:

With recent advancements in UAV based technology the use of airborne photogrammetry and LiDAR poses a new and effective approach for continuous, fast and efficient beach monitoring surveys. This paper aims to compare three platforms (a DJI Phantom Pro 4 using Ground Control Points, a DJI Matrice 200 with built in PPK allowing direct georeferencing and a DJI Matrice 600 with a Riegl Mini-VUX LiDAR system) in order to assess if they enable beach surveys to be performed efficiently, accurately and cost-effectively. A series of beach surveys were performed over a period of 6 months enabling the ability of each UAV surveying technique to be assessed for the identification and evaluation of trends in the changing topography of beaches and shorelines. The study area (Warnbro Sound, Western Australia) is an area that has experienced significant coastal change over the last 20 years as well as several serious weather events in the course of this research. The results show a significant positive bias of a consistent vertical offset to the ground surface by $4-9$ cm between the two image based systems in comparison to the LiDAR system. Although these height offsets are significant it is still within the accuracy required to perform successful beach surveys, and all systems were able to quantify the change of the beach shoreline in area (m^2) and volume (m^3).

1. INTRODUCTION

Coastal changes on larger scales and beach changes on smaller scale are natural phenomenon whereby sediment is either eroded away from or accreted to a coastal area. Erosion is a process where material is removed from a shoreline resulting in the retreat of the coastline and loss of land (Ghosh et al., 2014), while accretion occurs due to material being deposited on a shoreline, resulting in the creation of land and the advancement of coastline in a seaward direction (Gibb, 1978). Although this process is natural, due to a range of factors including rising sea levels, increased storm surges and man-made developments, the rate at which coastal and beach changes are occurring at coastlines is becoming more apparent (Ghosh et al., 2014; Splinter et al., 2014). A coastline can be defined as the line of contact between a water body (ocean or sea) and a land mass at an instant in time (Gens, 2010). It is currently estimated that erosion is occurring at over 70% of beaches worldwide (Fitton, 2018). Erosion can impact on coastlines by causing damage to real estate, infrastructure and ecosystems (Li & Gong, 2015). However, if coastal and beach monitoring is successfully implemented rehabilitation and prevention measures can be put in place to counteract the impact of coastal change.

Beach surveys have traditionally been performed using ground survey techniques such as Global Navigation Satellite Systems – Real Time Kinematic (GNSS-RTK) or total stations, where 3D point information is individually collected in a survey area (Delgado & Lloyd, 2004). Limitations with traditional survey methods are that there is a large degree of interpolation required to create Digital Elevation Models (DEM) (Uysal et al., 2015). Furthermore, they are time consuming, which limits the size of the areas that can be surveyed and subsequently increases the overall cost of the survey. Developments over the last decade in

Terrestrial Laser Scanning (TLS) and Mobile Laser Scanning (MLS) have overcome the high levels of interpolation in the creation of DEMs required by traditional surveying techniques. However, these techniques are still time consuming and can have a large impact on the environmentally sensitive areas being surveyed due to observations being required to be captured, using vehicles or by foot, in areas undergoing rehabilitation such as sand dunes and vegetated areas. Therefore, in this paper we will focus on airborne solutions only.

This paper aims to analyse the benefits and accuracy of using modern drone-based surveying techniques for beach monitoring. Through analysis of current commercially available UAV photogrammetry and UAV LiDAR systems the advantages, limitations and accuracy in obtainable spatial data can be investigated.

The paper is structured as follow: After related work is reviewed in section 2, the study area and the platforms utilised are introduced in section 3. After the processing pipeline is briefly introduced in section 4, the results will be presented in section 5. The paper will conclude with section 6.

2. RELATED WORK

Beach surveys can be performed using high resolution satellite imagery and remote sensing techniques (Splinter et al., 2014); however, these methods are more prominent for coastal monitoring, and therefore outside of the scope of this paper which focuses on high resolution beach monitoring.

UAV photogrammetry systems have successfully been utilised for data capture of beaches around the world with positive

---

* Corresponding author

success and accurate results being achieved. For instance, Gonçalves & Henriques (2015) assessed the viability and achievable accuracy of UAV photogrammetry for monitoring a spit of sand at the mouth of the Douro river in Cabadelo, Brazil. In this study a fixed wing UAV system was utilised to capture 367 images over a 1.30 km^2 area and at a flight height of 130 m which enabled a Ground Sample Distance (GSD) of 4.5 cm to be achieved. A number of Ground Control Points (GCPs) and Check Points (CPs) were placed around the survey area using GNSS-RTK. A RMSE of approximately 5 cm was identified for the UAV photogrammetry data collected over the sand surface, whereas an RMSE of approximately 3 cm was obtained over a neighbouring road surface. Further, the vertical accuracy of the UAV photogrammetry data was correlated to the accuracy of the GNSS-RTK survey, which is typically only accurate to 1-2 cm, as well as the systematic errors that are introduced when surveying over sand. Gonçalves & Henriques (2015) concluded that the use of UAV photogrammetry systems for topographic mapping was a massive breakthrough for the monitoring and study of morphological conditions in coastal areas, and that the ability to capture high resolution DEMs and orthomosaics with high spatial temporal resolutions can allow for an update of current coastal monitoring procedures.

A study performed by Drummond et al. (2015) assessed the ability of UAV photogrammetry systems to monitor armour stone movement in the Harrington breakwater in New South Wales, Australia. For this paper a fixed wing UAV platform equipped with GNSS-RTK was utilised and was able to survey the breakwater before and after the impact of a storm. The UAV photogrammetry survey was able to create orthomosaics and a 3D point cloud with the intention of monitoring armour stone movement in the breakwater. The point clouds created through the surveys comprised of 50 million elevation points, with a density of 80 points/m², which enabled the detection and tracking of the change of position of individual armour stones which formed the breakwater, as a result of storm damage. Drummond et al. (2015) could then successfully identify specific sections of the breakwater that required maintenance and repair.

In the same study a 1.5 km2 stretch of coastline along the Narrabeen-Collaroy Beach in Sydney, Australia was monitored using a fixed-wing UAV system. The stretch of beach was monitored before and after the impact of a storm capturing over 150 images with 80% overlap and a GSD of 4 cm. The use of a UAV system equipped with GNSS-RTK meant that GCPs were not required to be established through the survey area. However, a GNSS-RTK survey was performed simultaneously to the UAV photogrammetry survey to obtain CPs through the survey area. Drummond et al. (2015) were able to analyse the impact of the storm on the gradient of the beach by producing a high resolution orthoimage and dense point cloud. Through comparison of the collected UAV photogrammetric data against the GNSS-RTK surveys the accuracy of the UAV photogrammetry data could be identified. Both the GNSS-RTK and UAV photogrammetry surveys strongly agreed with one another and were able to identify a 6% change in gradient to the beach surface between the before and after storm surveys. This was obtained by overlaying the point clouds obtained prior and post storm and taking cross sections at various locations throughout the survey area.

On the other hand, UAV LiDAR is a relatively new technology, with commercially available systems only becoming available in the last 1 - 2 years. Thus, there has only been limited research

into the applicability of using UAV LiDAR for topographic surveys and even less research on the use of UAV LiDAR to perform beach surveys.

The use of UAV LiDAR for coastal monitoring was documented in (Assenbaum, 2018) for the purpose of identifying erosion and the impact that it was having on groundwater reserves in Perpignan, France. The study utilised a YellowScan Surveyors LiDAR System which was integrated with a multirotor UAV platform, which uses a Precise Point Kinematic (PPK) GNSS positioning system. This paper identified that the benefits of the UAV LiDAR survey, over photogrammetry surveys completed in the same area, were that accurate DTMs can be created, even in areas of vegetation, the fast speed to which the survey can be completed, and the reliability of captured data over weakly textured surfaces. The LiDAR survey was analysed against an RTK-GNSS survey over the coastal area and a test area of road to investigate the accuracy of the height component of the LiDAR point cloud. It was identified that the standard deviation in results obtained over the test road surface was 2.5 - 5 cm, while the survey performed over the coastal area resulted in a standard deviation of 9.5 cm in the height component. Assenbaum (2018) identified that the potential reason for the significantly larger standard deviation over the coastal area was in relation to the soft sand and the challenging surfaces being modelled. The research identified the high suitability of using UAV LiDAR for beach monitoring and proposed that with current regulations and feasible weather conditions coastal surveys of coastlines up to 10 km long could be performed in a single day.

While previous studies show the potential in using drones for beach monitoring, new and improved products require frequent assessment to identify potential improved performance for beach monitoring with drones.

3. STUDY AREA AND DATA COLLECTION

Surveys were performed using a DJI Phantom 4 Pro (P4P), a DJI Matrice 200 with a built in Loki GNSS receiver and equipped with a Zenmuse XT camera and a DJI Matrice 600 with a built in GNSS/AP20 IMU and equipped with a Riegl Mini LiDAR VUX-1UAV system. For the purpose of this analysis the P4P UAV platform was treated as the photogrammetry Aerial Triangulation (AT) dataset and involved the processing of the collected images with full ground control. The M200 platform was treated as the photogrammetry Direct Georeferencing (DG) dataset and no GCPs were used to process the obtained images. The Riegl platform was treated as the LiDAR data set. An overview of all platforms is provided in Table 1.

	P4P	M200/ Zenmuse XT	M600/Riegl
Sensor	1" CMOS	1" CMOS	NA
Resolution	24 MP	24 MP	100,000 laser pulses per second
Focal Length	8.8 mm	8.8 mm	NA
Image dimensions	4864 x 3648 pixel	5472 x 33648 pixel	NA
# of echoes	NA	NA	5 per laser signal

Table 1: Overview of data capturing platforms.

The primary study area is located in the Warnbro Sound in Safety Bay, Western Australia, which is located 54 km south of Perth. This particular study focused on the survey of a growing land mass (spit) that has formed in the Warnbro Sound due to high levels of accretion of sediment. A spit can be defined as a narrow coastal land formation and is frequently formed where the coast abruptly changes (see Figure 1).

Figure 1. Warnbro Sound Study Site (Dec 2017). Image taken from Google Earth

The study of the Warnbro Sound spit was completed between April and October 2018 and consisted of three survey epochs. All flights took place in the late morning hours between 10 a.m. and 12 p.m. The image-based systems were flown with an 80/80 overlap; the LiDAR system was flown with a 80/50 overlap. An overview with further details to each flight is provided in Table 2.

	Epoch 1	Epoch 2	Epoch 3
Date	26/04/18	07/08/18	23/10/18
Platform	P4P	P4P / Riegl Mini	M200, P4P, Riegl Mini
Area [km²]	0.029	0.108	App. 0.1
Flight height [m]	40 and 60	P4P: 80 Riegl Mini: 100	M200: 80 P4P: 80 Riegl Mini: 100
# flight strips	8	P4P: 8 Riegl Mini: 3	M200: 7 P4P: 7 Riegl Mini: 3
# cross strips	5	NA	NA

Table 2: Overview of data capture.

4. METHODOLOGY

4.1 Photogrammetric Aerial Triangulation (AT) method

The reference observations were performed as a GNSS-RTK survey using two Trimble R10 receivers (vertical accuracy of ±15 mm ± 0.5 ppm and horizontal accuracy of ± 8 mm ± 0.5 ppm). The base station receiver was set up over a Standard Survey Mark (SSM). The same SSM was utilised for each epoch to provide consistency in the collected GNSS observations of the UAV Ground Control Points (GCP) and Check Points (CP). Prior to each survey the quality of the SSM and station setup was verified against a neighbouring SSM.

For the first epoch survey, five GCPs were established at the centre and extremities of the survey area. For epoch 2 and 3 the number of GCPs were increased to 8 and 11, respectively, to account for the larger survey area.

For the processing of the images, the software product Pix4D was utilised. After the initial alignment of the images, GCPs were observed and a camera calibration was performed. After a successful camera calibration a dense point cloud / digital surface model (DSM) was created, and used to create an orthomosaic.

4.2 Photogrammetric Direct Georeferencing (DG) method

The same survey mark utilised to observe the GCPs and CPs was also used for the direct georeferencing of the M200. Post processing of the collected GNSS observations were performed using ASP Suite to identify the external orientation of each image. After the post processing of the GNSS/IMU data, the same software products utilised for the AT method were used to process the UAV imagery. The only difference being that the camera was self-calibrated as the Zenmuse XT was pre-calibrated in laboratory conditions.

4.3 LiDAR processing

The processing of the collected LiDAR data can be separated into three stages: (1) the processing of the GNSS and IMU data. (2) The processing of the GNSS/IMU data with the range measurements and (3) the photogrammetric processing of images captured with the integrated camera sensor in order to render the point cloud with colour information. Processing of UAV LiDAR was completed using RiProcess which was provided with the Riegl Mini VUX system.

4.4 DTM extraction

As changes in the terrain are important for beach monitoring, a DTM was required to be extracted from the DSM. For the DTM extraction, points not belonging to the terrain have to be classified and removed. The classification was performed on each 3D point cloud to classify surfaces and remove noise in the point clouds through the detection and removal of outlier points. Classification routines were utilised to filter and classify the point cloud into two surfaces, these being ground and non-ground points e.g. vegetation and structures.

The ground classification routine assigned a maximum terrain angle of 88 degrees. The maximum iteration angle between a point, its projection plane and the closest triangle vertex was set to 3 degrees and the maximum distance that a point could be located from the triangle plane was assigned as 0.7 m. The smoothing routine applies a maximum elevation change upwards and downwards to apply to a point of 0.4 m and a maximum elevation change downwards to a point. There are three height above ground classifications that were performed to classify point data based on heights $0 - 0.3$ m above the ground (low vegetation), $0.3 - 0.5$ m above the ground (medium vegetation) and $5 - 99$ m above the ground (high vegetation).

5. RESULTS

5.1 Image processing results

Overall the image processing results are satisfying considering a re-projection error of less than 1 cm for both datasets. Actually, those numbers are highly optimistic considering the RMS value of the GCPs of 9-22 mm. (see Table 3). The GCPs show relatively small vertical RMS values, however this contrasts with the vertical RMS of the CPs which are significantly larger $0.049 - 0.092$ m. Overall, we can conclude that the image processing was successful.

	Epoch 1	Epoch 2	Epoch 3	
Platform	P4P	P4P	P4P	M200
Processing method	AT	AT	AT	DG
Re-projection error (pixels)	0.158	0.191	0.174	0.190
Re-projection error (cm)	0.171	0.478	0.435	0.502
GCP RMS (m)	0.012	0.022	0.009	N/A
CP RMS (Z) (m)	0.067	0.092	0.049	0.064
Average point spacing (points/m2)	16.2	14.9	15.7	17.1

Table 3: Overview of image data processing.

The LiDAR point cloud were also successfully processed with no significant errors detected. The average point spacing of the LiDAR point cloud was calculated to be 60 points/m^2.

5.2 Profile comparison

Vertical cross sections were created over an area of the beach face. Figure 2 shows the location of the cross section which was created over a flat beach area with no vegetation or seaweed. Analysis was performed using the data obtained from epoch 3 where the P4P was treated as the photogrammetry (AT) data set, the M200 was treated as the photogrammetry (DG) data set and the Riegl Mini was treated as the LiDAR data set.

Figure 2. Location of the cross for the profile comparison without vegetation.

Figure 3 displays an analysis of the vertical cross sections created along the beach surface in the unclassified (DSM) and classified point cloud (DTM) for each technique. From the unclassified vertical cross sections, it can be observed that the photogrammetric point clouds are very noisy over the beach surface. The photogrammetry (AT) cross section (top) is the noisiest out of all the techniques, with elevation spikes of up to 0.3 m, while the photogrammetry (DG) cross section (middle) has elevation spikes of up to 0.15 m. In comparison the LiDAR cross section (bottom) is less noisy with elevation spikes of 0.05 m. From a comparison of the unclassified and classified/smoothed cross sections for each technique it can be seen that classification removed the elevation spikes and created a smoother surface. Each classified cross section does not appear to have been significantly affected by the elevation spikes that are visible in the unclassified point clouds.
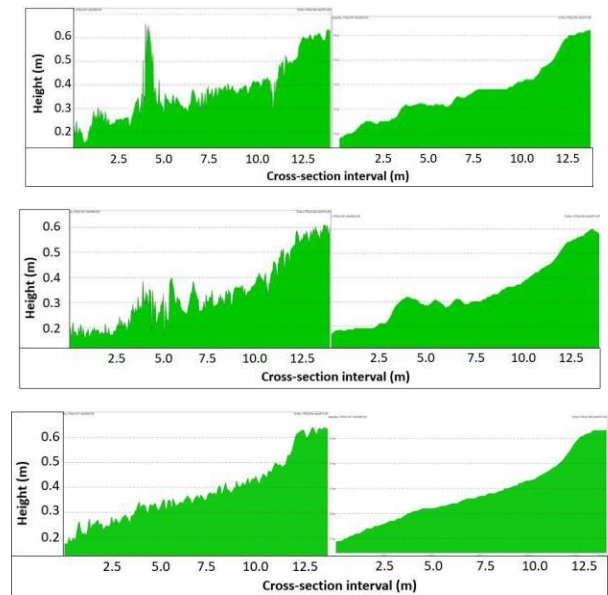
Figure 3. DSM (left) and DTM (right) profiles for the AT (top), DG (middle) and LiDAR (bottom) datasets of Epoch 3.

Figure 4 shows the elevation of the beach cross section for the photogrammetry (AT and DG) and LiDAR point clouds. There is a systematic trend in the heights of the photogrammetry (AT) cross section as it is consistently 4 – 9 cm higher than the LiDAR and photogrammetry (DG) cross section. Analysis of the photogrammetry (DG) heights identified a close agreement to the LiDAR classified point cloud with only small differences 0 – 5 cm in height. While the systematic trend of the AT dataset of 4 – 9 cm can be seen as significant, the differences between DG and LiDAR can be seen as not significant. However, the difference of 4 – 9 cm can be still ranked as acceptable due to the vertical threshold of 0.10 m defined by Gonçalves & Henriques, (2015) for detecting shape and volume changes in beaches.
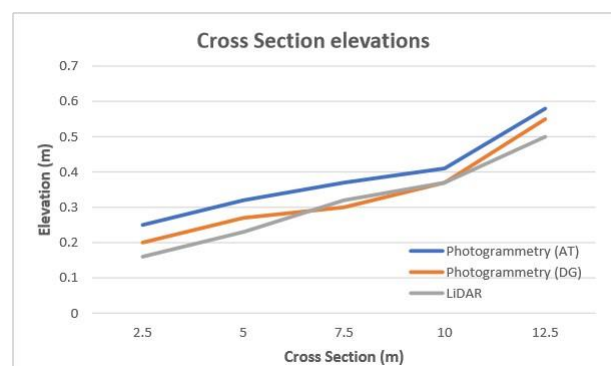
Figure 4: DTM profiles in comparison (AT blue, DG orange and LiDAR grey).

Next the profiles over a vegetated area as shown in Figure 5 will be discussed.
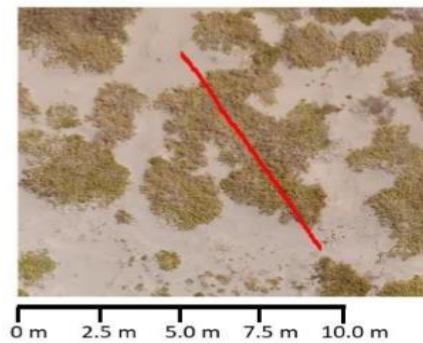
Figure 5. Location of the cross for the profile comparison with vegetation.

Figure 6 displays the vertical cross section created by the photogrammetry AT method (top) and the LiDAR method (bottom). The point cloud profiles are colour coded – purple points have been classified as ground points, and green points have been classified as points belonging to vegetation. Analysis of the vertical AT cross sections shows that this method was unsuccessful in penetrating the ground surface through the dense vegetation (red circles in the top figure). The lack of ground penetration of photogrammetry was expected. In contrast, it was expected that the LiDAR point cloud would be able to penetrate areas of vegetation. However, the success of the classification identified in Figure 8 is contrary to this theory and displays how the classification of the ground surface was unsuccessful through the vegetation (red circle in the bottom figure). This is due to the high density of the vegetation in this area, resulting in the LiDAR being unable to penetrate through the vegetation.
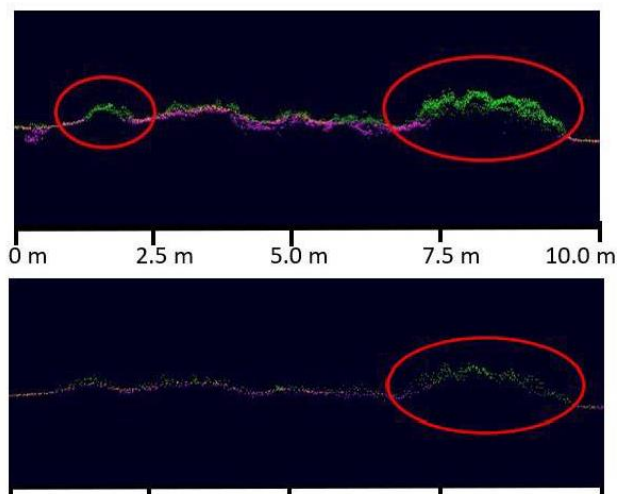

Figure 6 DSM profiles over a vegetation area for the AT (top) and LiDAR (bottom).

5.3 Assessment of vertical accuracy of AT, DG and LiDAR based on CPs

Next, we compare the photogrammetry (AT) and LiDAR UAV surveys from epoch 2. A point-based comparison was performed on the heights of the photogrammetry and LiDAR 3D point clouds against the heights of 81 CPs surveyed using GNSS-RTK. Table 7 displays an analysis of the minimum, maximum and average height differences, Root Mean Square Error (RMSE) and the Standard Deviation (STD).

	AT	LiDAR
Average dZ (m)	0.088	0.006
Minimum dZ (m)	0.033	-0.051
Maximum dZ (m)	0.202	0.122
RMSE (m)	0.092	0.029
STD (m)	0.027	0.028

Table 4: Comparison of the CPs (vertically).

A positive trend is suspected again in the AT dataset as the average dZ is close to 9 cm. In contrast the LiDAR dataset has an average dZ value of only 6 mm. While the STD of both datasets is comparable and below 3 cm indicating a good precision, the RMSE value of the AT dataset supports the speculation of an approximate 9 cm vertical error.

Figure 7 displays a histogram analysis of the height differences between the AT and LiDAR datasets against the GNSS-RTK CPs. From this Figure the positive systematic bias in the height differences can be observed for the AT dataset. It can be observed that there are no observations with a negative height difference to the GNSS-RTK CPs and the mean of the height differences is around 0.09 m. In contrast, the LiDAR dataset displays no systematic bias and has a mean close to 0 and an even number of negative and positive height differences. The LiDAR height differences display a normally distributed bell-shaped curve and indicates a higher precision in the observed height differences to the GNSS-RTK CPs.
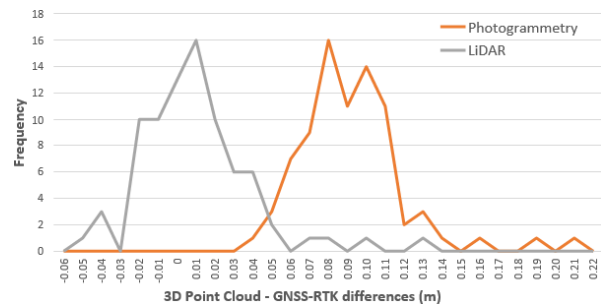

Figure 7: Histogram analysis of the height differences between the photogrammetry (AT) and LiDAR 3D point clouds against the GNSS-RTK CPs.

5.4 Point based comparison aerial triangulation (AT) vs direct geo-referencing (DG) vs LiDAR

This test compares the photogrammetry (AT), photogrammetry (DG) and LiDAR UAV surveys of epoch 3 against one another. It is more specifically a point-based comparison of the heights of the photogrammetry and LiDAR 3D point clouds against the heights of 92 CPs that were surveyed using GNSS-RTK.

	AT	DG	LiDAR
Average dZ (m)	0.042	0.058	-0.010
Minimum dZ (m)	-0.019	0.010	-0.073
Maximum dZ (m)	0.107	0.129	0.070
RMSE (m)	0.049	0.064	0.030
STD (m)	0.025	0.027	0.028

Table 5: Comparison of the CPs (vertically).

From Table 5 it can be observed that the LiDAR dataset has the highest accuracy out of the three techniques, which is identified

by the average dZ of -0.010 m and an RMSE of 0.030 m. A positive shift is suspected in the photogrammetry point clouds, which is identified by the large positive dZ averages of 4.9 cm (AT) and 5.8 cm (DG). The STD was less than 3 cm for each dataset, which identifies a good precision. The range in height differences (minimum to maximum dZ) is almost identical in the AT and DG datasets, however, due to the suspected positive vertical shift the maximum is approximately 2 cm larger in the DG dataset (0.129 m) in comparison to the AT dataset (0.107 m). The range in height differences is larger for the LiDAR dataset in comparison to the photogrammetry datasets, however, the LiDAR dataset has a much more even distribution of positive and negative height differences (-0.073 to 0.070 m).

The histogram analysis of the height differences (Figure 8) between the photogrammetry point clouds and the GNSS-RTK observations both identify the presence of a systematic error causing a positive bias in the height differences. The observed systematic bias in the photogrammetry datasets is largest for the DG dataset (yellow) which has a mean close to 6 cm, while the AT dataset (orange) is slightly lower with a mean of approximately 4 cm. The height differences between the LiDAR 3D point cloud (grey) and the GNSS-RTK observations identifies a small negative bias in the height differences with a mean close to -0.01 m. The LiDAR dataset obtained the highest accuracy out of the three techniques.
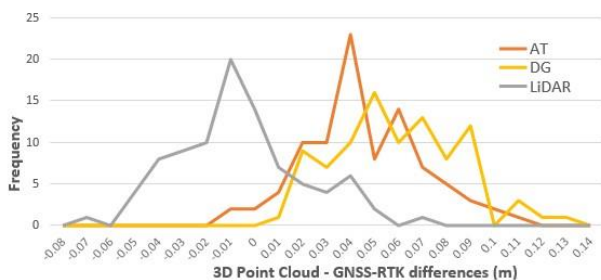

Figure 8: Histogram analysis of the height differences between the AT (orange), DG (yellow) and LiDAR (grey) 3D point clouds against the GNSS-RTK CPs.

5.5 Cloud based comparison aerial triangulation (AT) vs direct geo-referencing (DG) vs LiDAR

The final test compares photogrammetry (AT) and photogrammetry (DG) against the LiDAR point cloud of epoch 3. As the LiDAR did not exhibit a significant systematic bias in previous analysis it is used here as the reference dataset. Firstly, the height difference between DTMs is investigated. Figure 9 displays the histograms of the cloud-to-cloud distances between the LiDAR and AT (top) and the LiDAR and DG DTMs (bottom). All distances between the two surfaces are displayed in one direction (as positive differences). It can be observed from the histogram that there is a systematic trend resulting in a mean height difference of approximately 0.055 m in the LiDAR to AT comparison, while there is a 0.085 m systematic trend in the LiDAR to DG comparison. The distribution of the differences does not closely follow the Weibull distribution curve and there is an irregular trend identifiable in both histograms causing the distributions to be larger than the Weibull curve. The reader is referred to Nafidi et al. (2019) for an in-depth analysis of the Weibull distribution.
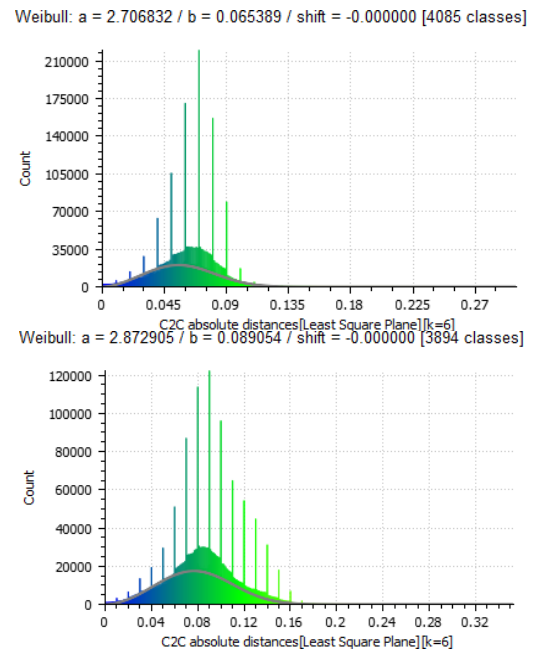

Figure 9: Distribution of the cloud-to-cloud distances between the LiDAR and AT (top) and the LiDAR and DG (bottom) DTMs plotted against the Weibull distribution

The comparison is repeated after the removal of the bias in order to compare the precision. The results are shown in Figure 10. Registration of the DTMs has resulted in a high correlation in differences for both the LiDAR to AT and the LiDAR to DG comparison. It can be observed that the distributions closely follow the Weibull curve indicating a high accuracy and precision between each set of DTMs. This indicates and reinforces the theory that the systematic trend in the photogrammetry dataset is a result of a positive and uniform shift in the heights of the 3D point cloud.
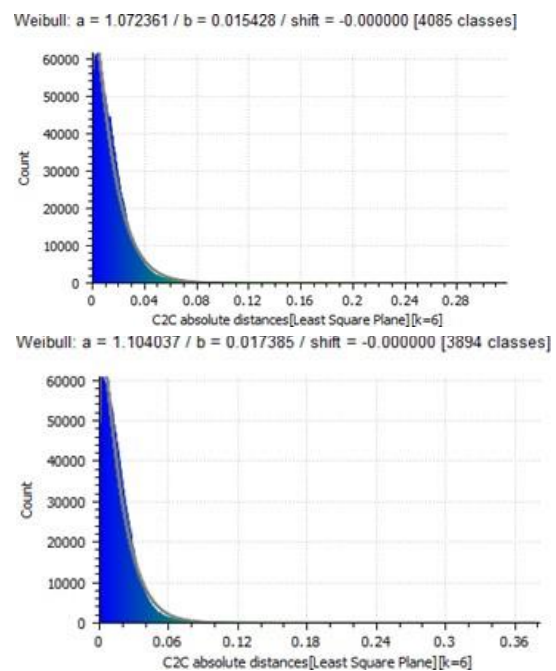

Figure 10: Distribution of the cloud-to-cloud distances between the LiDAR and AT dataset (top) and the LiDAR and DG dataset (bottom) plotted against the Weibull distribution.

Table 6 displays a statistical analysis of the mean, STD and unregistered and registered cloud-to-cloud analysis of the LiDAR and photogrammetry DTM comparisons. The cloud-to-cloud comparison of the DTMs identifies the positive bias in the DG and AT DTMs as the mean of the differences is 0.080 m for the DG comparison and 0.059 m for the AT comparison. The difference in mean between the DG and AT comparison identifies an error of 0.021 m between the two unadjusted datasets.

The mean of the distribution in differences improved significantly after removing the bias with the LiDAR to DG dataset improving by 0.063 m to 0.017 m and the LiDAR to AT distribution means improving by 0.044 m to 0.015 m. Improvements after removing the bias were also identified in the improvement in STD for both datasets. The effect of the registration further indicates that the systematic bias identified in the photogrammetry (DG) and (AT) datasets is a vertical shift in the 3D point clouds. Registration of the LiDAR and photogrammetry point clouds resulted in a strong correlation between the DTMs.

	With Bias	Bias removed	With Bias	Bias removed
	LiDAR vs DG	LiDAR vs DG	LiDAR vs AT	LiDAR vs AT
Mean (m)	0.08	0.017	0.059	0.015
STD (m)	0.03	0.017	0.023	0.016

Table 6: Statistical analysis of cloud-to-cloud height differences.

5.6 Detection of beach change

The beach change detection analysis was completed to demonstrate the concept that the DTMs and orthomosaics created using UAV photogrammetry and LiDAR were capable of identifying coastal change between epochs. After analysing the different sensors, the beach monitoring was performed using the following datasets: AT dataset for epoch 1, the AT as well as the LiDAR dataset for epoch 2, and the LiDAR dataset for epoch 3. The analysis of beach change was completed to identify changes between:

- Epochs 1 – 2 (AT_1 to AT_2)
- Epochs 2 – 3 (LiDAR_2 to LiDAR_3).

Beach erosion was most prominent between epochs 1 and 2 and is shown in Figure 11.
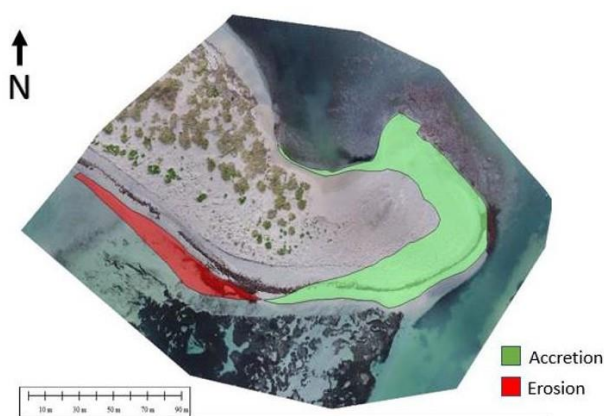

Figure 11: Coastline movement between epochs 1 and 2.

Table 7 quantifies the changes and analysis of the size of the area that had been accreted and eroded away between each

epoch. An area analysis performed on the erosion and accretion areas identified that there was 3,521 m^2 of accreted sediment and 1,255 m^2 of eroded sediment between epochs 1 and 2. Those values are most likely due to the heavy winter storms which led to heavy beach erosion in the areas in and around Perth. For instance (Barry, 2018) documented that storm activity in June 2018 caused severe erosion in Grace Darling Park in Lancelin, Western Australia causing the collapse of a gazebo into the ocean.

For epochs 2 to 3 the size of the accreted area is 281 m^2 while the size of the eroded area is 134 m^2. The size of the erosion and accretion areas between epoch 2 and 3 are significantly smaller than the erosion and accretion areas between epochs 1 and 2. This is most likely due to the reduced number of storms that occur between August and October as well as the time period between epochs 2 and 3 (75 days) being shorter than between epochs 1 and 2 (105 days). Another factor that would have influenced the size of the erosion and accretion areas between epochs 2 and 3 is the effect of the tide. As the epoch 1 and 2 surveys were performed at low tide the maximum area of beach face would have been visible. The epoch 3 survey was performed at low – mid tide which would have resulted in the ocean level being higher and subsequently covering a larger area of the beach surface. This would result in the accretion area being smaller than it otherwise would have been at low tide and the erosion areas being larger.

	Erosion (m^2)	Accretion (m^2)
Epochs 1 – 2 (26th of April – 9th of August)	1,255	3,521
Epochs 2 – 3 (9th of August – 23rd of October)	134	281

Table 7: Accretion and erosion between epochs

Further analysis of accretion and erosion in the study area was performed in relation to determining the volume of sediment change that has occurred between each epoch. The analysis was performed by calculating the volume difference between the DTMs created at each epoch. This analysis was performed between epochs 1 and 2 using the DTMs obtained from photogrammetry AT and between epochs 2 and 3 using both the photogrammetry AT and LiDAR DTMs. Table 8 displays the estimated volume of erosion and accretion detected between each epoch.

Epoch:	1 - 2	2 - 3	
Technique:	AT	AT	LiDAR
Erosion (m^3)	925.773	478.384	466.561
Accretion (m^3)	916.786	482.212	482.661

Table 8: Volume analysis of erosion & accretion between epochs.

From the volume analysis identified in Table 10 it can be observed that there was a significant amount of erosion (925.773 m^3) and accretion (916.786 m^3) between epochs 1 and 2. In contrast the amount of erosion and accretion was almost half that amount between epochs 2 and 3.

Through the analysis of the erosion and accretion volume estimates between epochs 2 and 3 for the photogrammetry (AT) and LiDAR datasets it can be observed that the volume estimate for the accretion was nearly identical to one another with a difference of only 0.5 m^3. The volume analysis of the eroded

surface was slightly larger (10 m^3), however this is still very similar and indicates a high correlation in the analysis of beach changes possible with the LiDAR and photogrammetry techniques. This is a significant analysis as it identified that even though there were observed positive systematic trends in the photogrammetry (AT) datasets the volume estimates agreed with the more accurate LiDAR dataset. The volume analysis subsequently suggests that both the photogrammetry (AT) and LiDAR UAV techniques are capable of detecting similar amounts of beach change.

6. CONCLUSION

The goal of this paper was to assess the effectiveness of UAV based surveying techniques when performing beach surveys and the identification of trends in beach changes. The study performed an analysis of UAV photogrammetry and LiDAR surveying to assess the accuracies, benefits and limitations of each technique. Once the accuracy of each technique was assessed a beach monitoring survey could be performed to identify how accurately each technique could identify the presence of erosion and accretion over time.

This research concluded that UAV LiDAR was the most suitable technique for performing beach surveys. The consistency in the results obtained in the validation analysis at the Warnbro Sound beach site identified a high correlation between the LiDAR and the ground truth observations. It was identified that the UAV LiDAR platform was able to penetrate areas of high vegetation, however it was not as successful in the penetration of low dense vegetation.

However, the coastal monitoring survey analysis performed using both the LiDAR and photogrammetry techniques identified that both survey methods were capable of identifying shoreline movement and detecting elevation changes to the beach face over time. The erosion and accretion volume analysis performed using photogrammetry and LiDAR identified a similar level of erosion and accretion, indicating that both methods are highly suitable for monitoring beach changes.

ACKNOWLEDGEMENTS

REFERENCES

Assenbaum, M. (2018). Monitoring coastal erosion with UAV lidar. GIM International, 32. DOI: 10.1016/j.GIM.2018.04.03

Delgado, I. & Lloyd, G. (2004). A simple low cost method for one person beach profiling. Journal of Coastal Research, 20, 1246-1252. DOI:10.2112/03-0067R.1

Barry, H. (2018). Premier Lancelin beachfront closed as storm damage threatens gazebo collapse. Retrieved from https://www.watoday.com.au/national/western-australia/premier-lancelinbeachfront-closed-as-storm- damage-threatens-gazebo-collapse-20180603-p4zj6k.html

Drummond, C.D., Harley, M.D., Turner, I.L., Matheen, A.N.A., Glamore, W.C. (2015). UAV Applications to coastal engineering. Australasian Coasts & Ports Conference 2015.

Fitton, J.M., Hansom, J.D. & Rennie, A.F. (2018). A method for modelling coastal erosion risk: the example of Scotland. Natural Hazards, 91. DOI: 10.1007/s11069-017-3164-0

Fuad, N.A., Majid, Z.M., Darwin, N., Ariff, M.F.M., Idris, K.M. & Yusoff, A.R. (2018) Accuracy evaluation of digital terrain model based on different flying altitudes and conditional of terrain using UAV LiDAR technology. IOP Conf. Series: Earth and Environemntal Sciences 169. DOI: 10.1088/1755-1315/169/1/012100

Gens, R. (2010). Remote sensing of coastlines, extraction and monitoring. International Journal of Remote Sensing, 31, 1819 – 1836. DOI: 10.1080/01431160902926673

Ghosh, M.J., Kumar, L., & Roy, C., (2014). Monitoring the coastline change of Hatiya Island in Bangladesh using remote sensing techniques. ISPRS Journal of Photogrammetry and Remote Sensing, 101. DOI: 10.1016/j.isprsjprs.2014.12.009

Gibb, J.G., (1978.) Rates of coastal erosion in New Zealand. NZ Journal of Marine and Freshwater Research 12(4), 429 – 456.

Gonçalves, J.A., & Henriques, R., (2015). UAV photogrammetry for topographical monitoring of coastal areas. ISPRS Journal of Photogrammetry and Remote Sensing, 105, 101 - 111. DOI: 10.1016/j.isprsjprs.2015.02.009

Li, W. & Gong, P. (2016). Continuous monitoring of coastline dynamics in Western Florida with a 30-year time series of Landsat imagery. Remote Sensing of Environment, 179, 196 – 209. DOI: 10.1016/j.rse.2016.03.031

A. Nafidi, M. Bahij, B. Achchab, R. Gutiérrez-Sanchez (2019). The stochastic Weibull diffusion process: Computational aspects and simulation. Applied Mathematics and Computation, 348. DOI:/10.1016/j.amc.2018.12.017.

Splinter, K.D., Carley, J.T., Golshani, A. & Tomlinson, R. (2014). A relationship to describe the cumulative impact of storm clusters on beach erosion. Coastal Engineering, 83, 49 – 55. DOI: 10.1016/j.coastaleng.2013.10.001

Uysal, M., Toprak, A.S. & Polat, N. (2015). DEM generation with UAV Photogrammetry and accuracy analysis in Sahitler hill. Measurement: Journal of the International Measurement Confederation, 73. DOI: 10.1016/j.measurement.2015.06.010